



HAL
open science

Phase contrast micro-tomography and morphological analysis of a short carbon fibre reinforced polyamide

F. Cosmi, A. Bernasconi, N. Sodini

► **To cite this version:**

F. Cosmi, A. Bernasconi, N. Sodini. Phase contrast micro-tomography and morphological analysis of a short carbon fibre reinforced polyamide. *Composites Science and Technology*, 2010, 71 (1), pp.23. 10.1016/j.compscitech.2010.09.016 . hal-00702318

HAL Id: hal-00702318

<https://hal.science/hal-00702318>

Submitted on 30 May 2012

HAL is a multi-disciplinary open access archive for the deposit and dissemination of scientific research documents, whether they are published or not. The documents may come from teaching and research institutions in France or abroad, or from public or private research centers.

L'archive ouverte pluridisciplinaire **HAL**, est destinée au dépôt et à la diffusion de documents scientifiques de niveau recherche, publiés ou non, émanant des établissements d'enseignement et de recherche français ou étrangers, des laboratoires publics ou privés.

Accepted Manuscript

Phase contrast micro-tomography and morphological analysis of a short carbon fibre reinforced polyamide

F. Cosmi, A. Bernasconi, N. Sodini

PII: S0266-3538(10)00373-8
DOI: [10.1016/j.compscitech.2010.09.016](https://doi.org/10.1016/j.compscitech.2010.09.016)
Reference: CSTE 4819

To appear in: *Composites Science and Technology*

Received Date: 24 March 2010
Revised Date: 15 September 2010
Accepted Date: 25 September 2010

Please cite this article as: Cosmi, F., Bernasconi, A., Sodini, N., Phase contrast micro-tomography and morphological analysis of a short carbon fibre reinforced polyamide, *Composites Science and Technology* (2010), doi: [10.1016/j.compscitech.2010.09.016](https://doi.org/10.1016/j.compscitech.2010.09.016)

This is a PDF file of an unedited manuscript that has been accepted for publication. As a service to our customers we are providing this early version of the manuscript. The manuscript will undergo copyediting, typesetting, and review of the resulting proof before it is published in its final form. Please note that during the production process errors may be discovered which could affect the content, and all legal disclaimers that apply to the journal pertain.



**PHASE CONTRAST MICRO-TOMOGRAPHY AND MORPHOLOGICAL
ANALYSIS OF A SHORT CARBON FIBRE REINFORCED POLYAMIDE**

F. Cosmi^a, A. Bernasconi^b, N. Sodini^c

^a Università degli Studi di Trieste, Dipartimento di Ingegneria Meccanica e Navale, via

A. Valerio 10, 34127 Trieste, Italy, e-mail: cosmi@units.it

^b Politecnico di Milano, Dipartimento di Meccanica, Via La Masa 1, 20156 Milano,

Italy

^c Sincrotrone Trieste, Area Science Park, Basovizza, Trieste, Italy

ABSTRACT

The mechanical properties of components made of short fibre reinforced composites, generally obtained by injection moulding, are strongly linked to fibre orientation. Therefore, it is of great importance to be able to verify the results of manufacturing process simulations obtained by commercial software. From the experimental point of view, the definition of carbon short fibre structure within a polymeric matrix in a micro-tomography is a non-trivial task, as the X-rays absorption properties of the two phases are very similar. This paper presents how this problem was overcome by using phase contrast imaging techniques. High resolution fibre structure reconstructions could therefore be obtained. The reconstruction of a large sample volume by overlapping of successive tomographies was also discussed. Moreover, this work shows that the anisotropy identification techniques based on morphological parameters, previously introduced by some of the Authors for short glass fibre

reinforced polymers, can also be adopted for fibre arrangement identification in this type of materials.

KEYWORDS: A. Short-fibre composites, A. Carbon fibres, A. Polymer-matrix composites, C. Anisotropy, D. Phase contrast micro-tomography.

1. INTRODUCTION

The recent rapid growth in structural parts applications of glass or carbon SFRP (Short Fibre Reinforced Polymers), especially in the automotive field, leads to an increasing need for a better understanding of their mechanical properties, which strongly depend on fibre arrangement and orientation within the polymeric matrix [1-4].

The manufacturing process, usually by injection moulding, determines the reinforcement final arrangement by:

- crushing the fibres and thus inducing a non uniform fibre length distribution and
- determining the melt polymer flow profile and the consequent reinforce final orientation [5-6].

Since different software exist that simulate the process, there is a special need to confirm these predictions by means of experimental tests.

Definition of short reinforce fibre structure within the matrix is nontrivial, due to several factors including small fibre dimensions, high numerosity and scattering of fibre directions even when a preferred orientation can be identified. A review of the usual methods is discussed in [7]. The most common destructive method consists in the analysis of the elliptic traces in several sections of the sample, from which the orientation of each single fibre can be inferred [8,9]. A non-destructive definition of the sample three-dimensional internal structure can be obtained by X-ray micro-Computed Tomography (micro-CT). The sample is placed on a rotating table and several

projections are acquired at different angles over 180 degrees. Successively, the radiographic images are combined using well-known algorithms, so that the internal 3D microstructure of the sample can be identified. Several morphologic parameters characterizing the material can be then evaluated from the reconstructed volumes. Again, a common approach consist in the evaluation of each single fibre geometry within the matrix [10].

Obviously, all these single-fibre approaches are only possible in case of relatively small number of reasonably large fibres, compared with sensor's resolution. Recently, some of the Authors have introduced the use of a global parameter, the Mean Intercept Length (MIL) for fibre arrangement identification, thus overcoming the fibre numerosity problem. Characterization of anisotropy by MIL, commonly utilized in biomechanics and geology, was adopted for SFRP samples. In this way, it was possible to identify local preferred fibre directions and anisotropy degrees in glass fibre reinforced thermoplastic polymers [7,11,12].

It must be pointed out that in conventional micro-CT, images are obtained from the attenuation coefficient map of the sample and structure detection is possible only if the density of fibre and matrix differ sufficiently. However, at 20 keV, the linear absorption coefficient of carbon is 0.75 cm^{-1} while the linear absorption coefficient of polyamide is 0.768 cm^{-1} , so that, given the small difference between the constituents X-ray absorption properties, carbon fibre distribution detection within a polymeric matrix is generally not possible with conventional X-ray sources.

This problem can be overcome by using information from phase shifts occurring in X-rays going through different material phases, which can be retrieved when high spatial coherence sources, i.e. synchrotron light, are used [13]. The adoption of PHase

Contrast (PhC) imaging techniques enhances the visibility of fibre borders even in case of small diameters, so that materials with very similar absorption index can be separated, like carbon fibre immersed in a polymer matrix. Recently, some results in this direction have been obtained for continuous fibre reinforced composites [14,15].

In this work, we present some new results in fibre structure identification, obtained by applying PhC techniques and the MIL morphology characterization method in a polymeric material reinforced with 30% weight short carbon fibre (PA66-CF30).

2. MATERIAL

Two samples, *carb1* and *carb2*, were obtained in the fillet and in the central part respectively of a longitudinally injected ISO 527 type 1A specimen, as shown in Fig.1. The specimen, $4 \times 10 \text{ mm}^2$ in section, was made of PA66-CF30, a thermoplastic polymeric matrix composite reinforced with 30% weight short carbon fibre. Nominal diameter of fibre was 7 microns. Fibre length followed a Weibull distribution with a weighted average of 350 microns and a maximum value of 750 microns. In the same Fig.1, the reference frame used in this work is indicated: the slices, sample sections in the x - y plane attained by micro-tomography, are stacked along the z direction to obtain the 3D reconstructions.

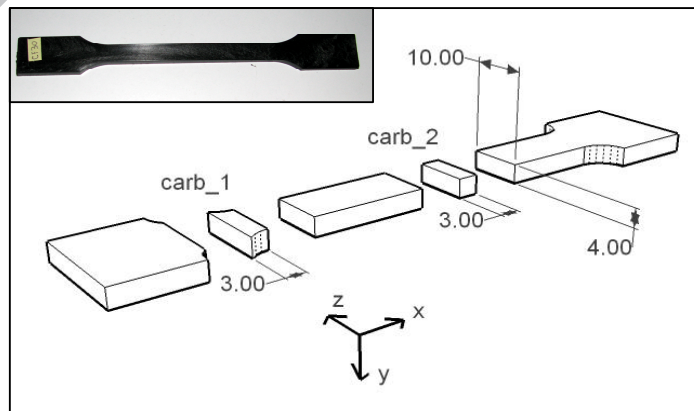


Figure 1: Samples position within the ISO 527 specimen (dimensions in mm)

Similarly to head injected plates, the expected fibre orientation is parallel to the injection direction in the *shell* layer, near the mould wall, while in the central *core* layer fibre distribution will be more complex and dictated by the velocity profile of mould filling flow, as it appears in Fig.2, where a clear difference in the fibre pattern in a portion of the cross section of the specimen, as reconstructed by micro CT, is shown.

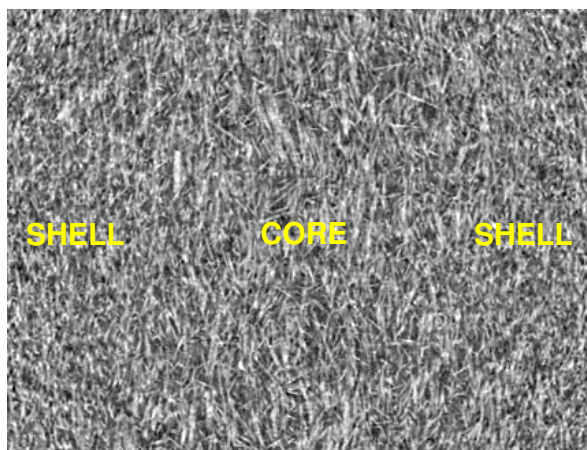


Figure 2: Micro-tomographic section, or slice, of the *carb2* sample (329 x 430 pixel², 9 microns resolution).

3. METHODS

3.1 Synchrotron radiation phase contrast micro-tomography

Synchrotron Radiation (SR) is an electromagnetic radiation, whose energy spectrum extends from visible light up to X-rays, emitted by electrons when they are deviated by magnetic fields. The peculiar characteristics of high brilliance and coherence make SR a powerful tool of investigation in different research fields. For our experiments we used the SR available at the SYRMEP beamline of the Elettra light source consisting in a monochromatic, laminar shaped X-ray beam with energy tunable between 8.3 keV and 35 keV.

Radiography with conventional X-ray generators is based on the absorption properties of the sample: the image contrast is produced by a variation of density, a change in composition or thickness and is based exclusively on the detection of the amplitude variation of the transmitted X-rays. Its main limitation is the poor intrinsic contrast for samples with low atomic number (i.e. the case of “soft matter”, like PMMA and carbon). On the contrary, the “phase sensitive imaging techniques” are based on the observation of the phase shifts produced by the object on the incoming wave [13]. In this case contrast arises from interference between parts of the wave front having experienced different phase shifts originated by the sample, as shown in Fig.3. Objects with negligible X-ray absorption can be visualized with high effectiveness by means of these methods.

In general, phase information can be accessed if the X-ray source has a high spatial coherence as for SR facilities, like ESRF in Grenoble (France) or Elettra, Trieste (Italy). Several approaches for phase-sensitive radiology have been recently reported [16]. Among these, the PHase Contrast (PHC) radiography has a quite simple operation: the PHC set-up is the same of conventional radiography with the difference that the detector is positioned at a certain distance d from the sample [17,18]. The choice of d depends on the size a of the feature to be identified, measured perpendicularly to the beam direction and on the X-ray wavelength (λ). In the edge detection regime ($d \ll a^2/\lambda$), images can be directly used to extract morphological information in the sample. Larger values of d lead to the holography regime ($d \approx a^2/\lambda$), where the local phase can be obtained.

In the PHC images, the pattern produced by phase contribution is simply superimposed to the absorption image and helps to strongly enhance the visibility of details, the phase boundaries being outlined by a black-white line.

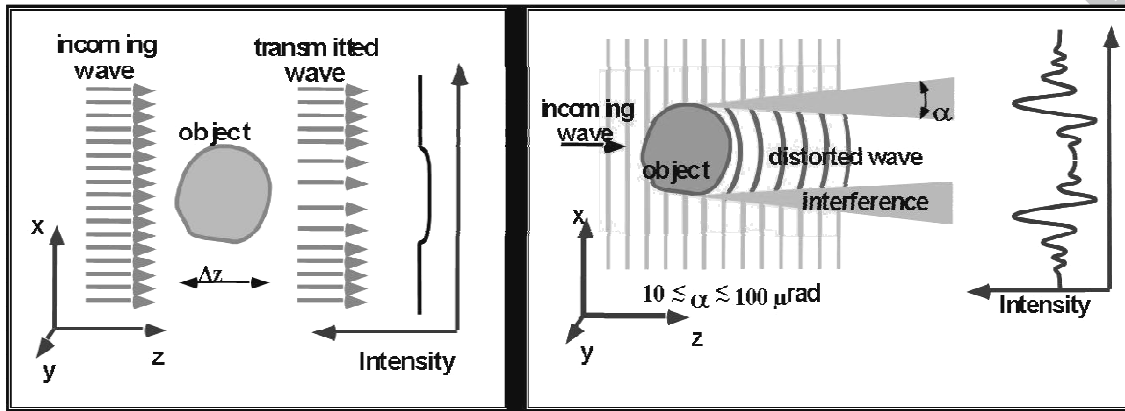


Figure 3: X-rays impinging the sample: absorption(left) and phase shifts (right) effects.

PHC techniques can be applied to planar radiography as well as to X-ray micro-CT. A schematic view of the experimental set-up used for our experiments at the SYRMEP beamline is shown in Fig.4.

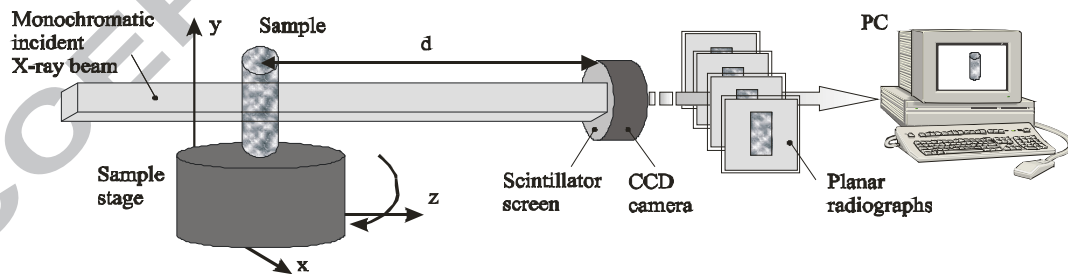


Fig. 4. Schematic view of the experimental set-up.

Images taken at $d = 1 - 2$ cm reproduce the absorption configuration. A distance of A distance of 15 cm has been determined for the PHC technique, according to the

criteria defined above. The X-ray energy selected for the experiments was 12 keV. During the data acquisition the sample is rotated from 0° to 180° around an axis perpendicular to the incident beam and projection images are recorded at the different rotation steps.

For each tomography set, 1440 projections of the sample were acquired at equally spaced rotation angles over the total rotation trip. The detector system used at the beamline is a 12bit water-cooled 4008×2672 pixels CCD camera. The camera spatial resolution corresponds to an effective pixel size of 9×9 microns² (Fig.5).

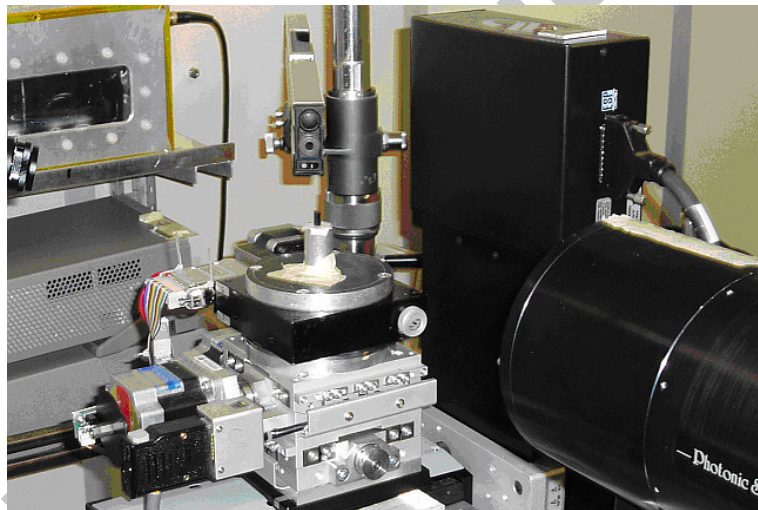


Fig. 5. Set-up used for the XMT experiments.

The reconstruction of the tomographic slices was performed applying a software code written in IDL language [19] and based on the filtered back-projection algorithm [20]. The reconstructed 2D image slices are visualized via the software ImageJ [21] and for 3D rendering commercial software VGStudio Max 2.0 was used.

As shown in Fig. 1, each sample is 10 mm in the z direction, while the beam section is approximately 6.5 mm high. Therefore, in order to reconstruct the entire sample

image, two successive tomographies were carried out for each sample (*carb1A*, *carb1B* and *carb2A*, *carb2B* respectively) as discussed in detail in the following Section 4.1.

3.2 Mean Intercept Length

As already discussed in the Introduction, single-fibre approaches for fibre orientation identification had to be ruled out, given numerosity and small dimensions of fibre in our samples. Instead, a global approach was applied using the Mean Intercept Length (MIL), as recently introduced by some of the Authors for short glass fibre reinforced polyamide [7].

Mean Intercept Length (*MIL*), defined as the average distance along a certain direction between the two phases of a material, is computed by placing a grid of parallel segments (of total length L and oriented along a direction indicated by the angle θ) on the Volume of Interest (VOI) image in the 3D reconstruction and by counting the number $I(\theta)$ of fibre to matrix transitions:

$$MIL(\theta) = \frac{L}{I(\theta)}. \quad (1)$$

A 3D polar diagram representing the two-phase structure properties can be then obtained by spanning a sufficient number of directions θ .

The *MIL* locus becomes a polygon in case of fibre organized along a finite number of directions [22,23]. On the contrary, in short fibre reinforced composites fibres are dispersed along all directions even when preferred orientations are present, so that the 3D *MIL* locus can be approximated by an ellipsoid [7,11,12] and a compact tensor notation can be used to define fibre arrangement properties. In the second order *MIL fabric tensor* thus defined, eigenvectors correspond to the principal directions of the anisotropic structure, while the normalized eigenvalues H_i can be considered a measure

of fibre distribution along these directions. An Index of Anisotropy IA can also be defined:

$$IA = 1 - \text{MIN}(H_i) / \text{MAX}(H_i) \quad (2)$$

so that $IA = 0$ in case of perfect isotropy and $IA = 1$ at the opposite end. *MIL* analyses have been performed using the freeware software Quant3D [24].

The 3D micro-CT reconstructions consist of 8-bit greyscale images so that a segmentation is necessary for *MIL* computations, which require the definition of two phases. This is usually a crucial procedure and more so in our case. In fact, commonly used filters already implemented in Quant3D software, like the Iterative filter described in [25] or FWHM (Full Width/Half Max) method, which chooses the midpoint greyscale between the maximum and minimum in the data set [26], could not be employed because our imaging technique was based on phase contrast besides grey tone modulation and could not be linked to quantitative information about sample composition. The use of the PHC techniques also allowed to compensate for the low resolution of the CCD sensor (9 μm) compared with the average fibre diameter (7 μm). Since PHC enhances the fibre edges, the corresponding pixels will appear in a shade of grey lighter than the matrix ones and the usual filters lead to an overestimation of fibre content. We overcame this problem by computing the threshold value yielding the expected volumetric fibre fraction (Fibre Volume/Total Volume, FV/TV) on the entire sample reconstruction and using it for all the VOIs extracted from the same reconstruction. The volumetric fibre fraction of 0.2135 for a PA6CF30 was evaluated from the weight fraction and the nominal densities of the fibres and the matrix. For example, the effect of the different filters on segmentation of reconstruction *carbIA* is shown in Table 1 and, visually, in Fig. 6.

Table 1: Effect of different filters on identification of fibre volume fraction (FV/TV) of sample *carb1A*. Expected value $FV/TV = 0.2135$, from fibre weight percentage.

Filter	Iterative	FWHM	Our method
<i>Threshold</i>	119	127	152
<i>FV/TV</i>	0.4767	0.3958	0.2111

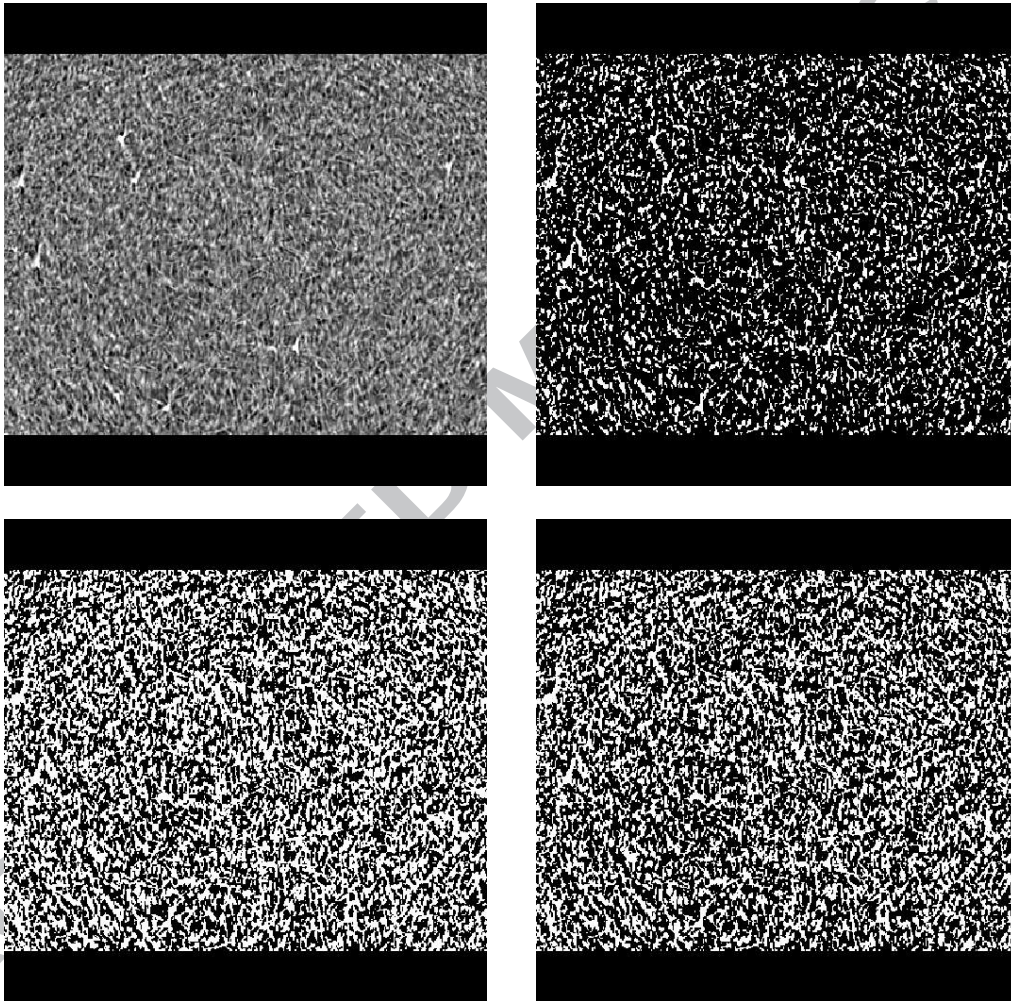


Fig. 6. Segmentation – 8 bit slice: original greyscale (left up), same image processed with our method (right up), with Iterative filter (left down) and FWHM filter (right down).

4. RESULTS

4.1 Image overlap

As already mentioned, two tomographies were carried out for each sample, as shown schematically in Fig. 7 for sample *carb2*. The first micro-tomographic image, *carb2A*, consists of 674 slices corresponding to 6.1 mm, the second, *carb2B*, is made of 695 slices, covering 6.3 mm. In the same Fig. 7 the overlap zone, 311 slices (2.8 mm), is also highlighted.

First of all, in order to be able to use the results obtained from two different tomographic scans (i.e. *carb2A* and *carb2B*) of the same sample (*carb2*), we verified the good agreement of *MIL* measures (eigenvalues and anisotropy index) in three control VOIs representing the same regions in different reconstructions of sample *carb2*. For this purpose we analyzed two volumes in the shell layer (40 and 80 pixel side) and one volume in the core region (30 pixel side) of the overlapping zone, as shown in Fig. 7.

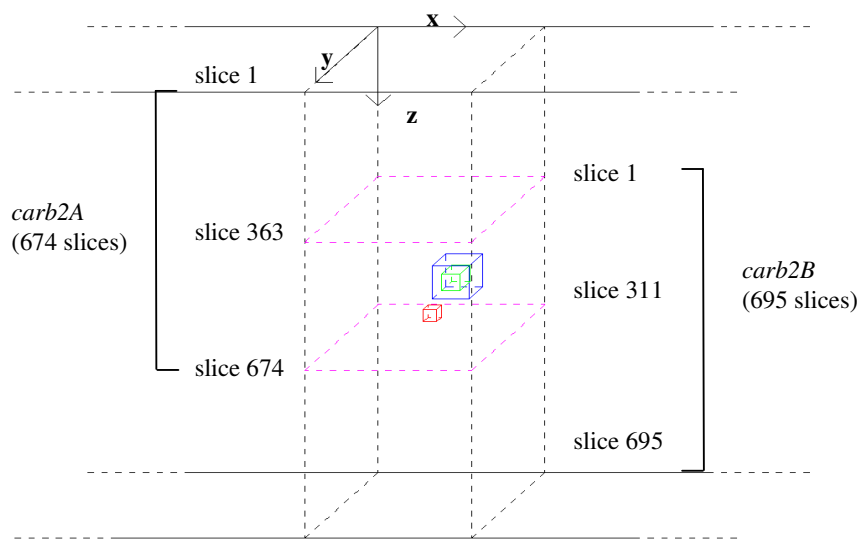


Figure 7: Sample *carb2* tomographies overlap and location of control VOIs: 40 pixel side (green) and 80 pixel side (blue) VOIs in the shell layer, 30 pixel side (red) VOI in the core layer.

It must be pointed out that the precision of the motors used to move the sample is in the order on the tenth of a millimetre, so that knowledge of the sequence of movements between the first and the second tomography does not guarantees alone an accurate overlap of the tomographies. Therefore, achieving an accurate identification of the overlap zone required some degree of attention and could only be performed manually, taking advantage of the presence of geometrical irregularities due to the sample cutting and of clearly recognizable fibre aggregations (see Fig. 8 as an example). Eight such structures were used for reconstruction overlap. These elements were clearly recognizable in the different tomographies, where they appeared to be similar but not identical. This is due to the nature itself of tomography as representation of a volume by a sequence of stacked parallel equidistant slices: it is in fact highly improbable to obtain perfectly coincident slices in two different tomographies, while it is more likely to get corresponding slices that are less distant from each other than the slice spacing (9 microns in our case).

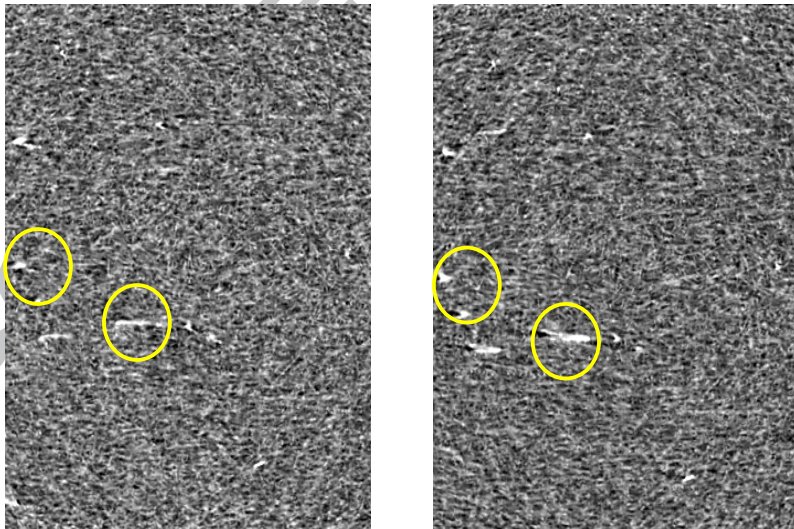


Figure 8: Two slices of the same region obtained in two different reconstructions, where some of the elements clearly recognizable as similar are highlighted.

The control VOIs morphological characterization was performed with Quant3D software [24,25]. The *MIL* eigenvalues H_i and the Index of Anisotropy IA reported in Tab. 2 are obtained from the average of 5 *MIL* fabric tensor evaluations.

Table 2: *MIL fabric tensor* eigenvalues, H_i , and Index of Anisotropy, IA , in the overlap control VOIs.

	<i>Carb_2A</i> <i>shell</i> (40 pixel)	<i>Carb_2B</i> <i>shell</i> (40 pixel)	<i>Carb_2A</i> <i>shell</i> (80 pixel)	<i>Carb_2B</i> <i>shell</i> (80 pixel)	<i>Carb_2A</i> <i>core</i> (30 pixel)	<i>Carb_2B</i> <i>core</i> (30 pixel)
H_1	0.45	0.46	0.45	0.46	0.36	0.36
H_2	0.33	0.32	0.33	0.22	0.34	0.34
H_3	0.22	0.22	0.22	0.22	0.30	0.30
IA	0.50	0.52	0.50	0.52	0.14	0.15

Software parameters used were: 513 equispaced directions, each with an initial random rotation, *dense vectors* sampling and a 1500 lines measuring grid [26]. As expected, all the *shell* layer control VOIs exhibit a strong alignment of fibres along the x direction, while the preferred orientation in the *core* layer is along z , as shown in Tab.3.

Table 3: Squares of the directional cosines of the MIL *fabric tensor* first eigenvector in the overlap control VOIs

	<i>Carb_2A</i>	<i>Carb_2B</i>	<i>Carb_2A</i>	<i>Carb_2B</i>	<i>Carb_2A</i>	<i>Carb_2B</i>
H_1	<i>shell</i> (40 pixel)	<i>shell</i> (40 pixel)	<i>shell</i> (80 pixel)	<i>shell</i> (80 pixel)	<i>core</i> (30 pixel)	<i>core</i> (30 pixel)
$\cos^2(\alpha)$	0.9994	0.9998	0.9995	0.9995	0.0709	0.0661
$\cos^2(\beta)$	0.0002	0.0002	0.0004	0.0003	0.0003	0.0055
$\cos^2(\gamma)$	0.0004	0.0000	0.0001	0.0001	0.9288	0.9284

4.2 Fibre arrangement identification results

Three series of measurements were performed on 30 pixel side VOIs extracted from each sample *carb1* and *carb2* reconstructions. The Index of Anisotropy was evaluated as the average of 15 computations, using 513 equispaced directions, initial random rotation, *dense vectors* sampling and 1500 lines measuring grid as Quant3D software parameters [26]. The first series of measurements, VOIs aligned in the y direction, was used to assess the extent of the *core* layer. These VOIs are shown in blue in Fig. 9 (the green VOI is the one also used for tomographies overlap control). Results are shown in Fig. 10.

Changes along the specimen width in the core layer were highlighted by the second series of measures, in the z direction (red VOIs in Fig. 9). Given the extension of the examined region, VOIs come from two tomographies overlap:

- in the case of sample *carb1*, slices from 15 to 495 belong to tomography *carb1A*, the successive to *carb1B*;

- in the case of sample *carb2*, slices from 15 to 645 belong to tomography *carb2A*, the successive to *carb2B*.

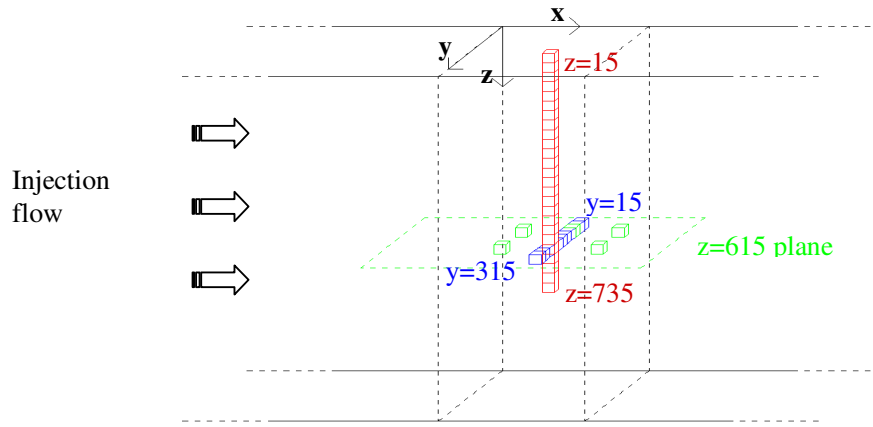


Figure 9: VOIs centre position – slice spacing : 9 microns

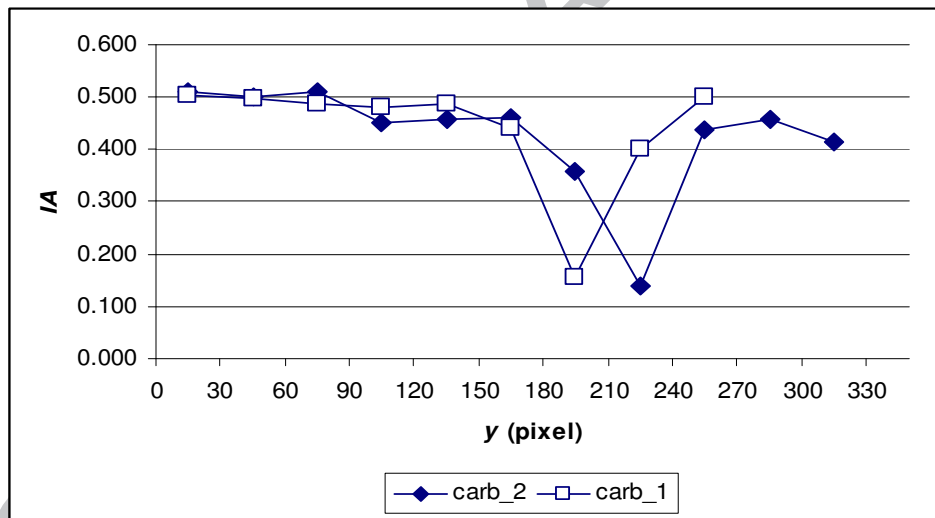


Figure 10: Index of Anisotropy, IA , along y direction (VOIs centre position in pixel)

Results are shown in Fig. 11. Different fibre arrangements are detectable between the fillet, *carb1*, and the central, *carb2*, sample.

The third series of measures was performed on sample *carb2* and was aimed at the evaluation of local changes in both the *core* and *shell* region. All VOIs had their centre

in the plane defined by slice 21 (these VOIs are shown in green in Fig. 9). For clarity, VOIs positions ($1_C, 2_C, 3_C$ in the *core* layer and $1_S, 2_S, 3_S$ in the *shell* layer) are depicted on slice 21 in Fig. 12.

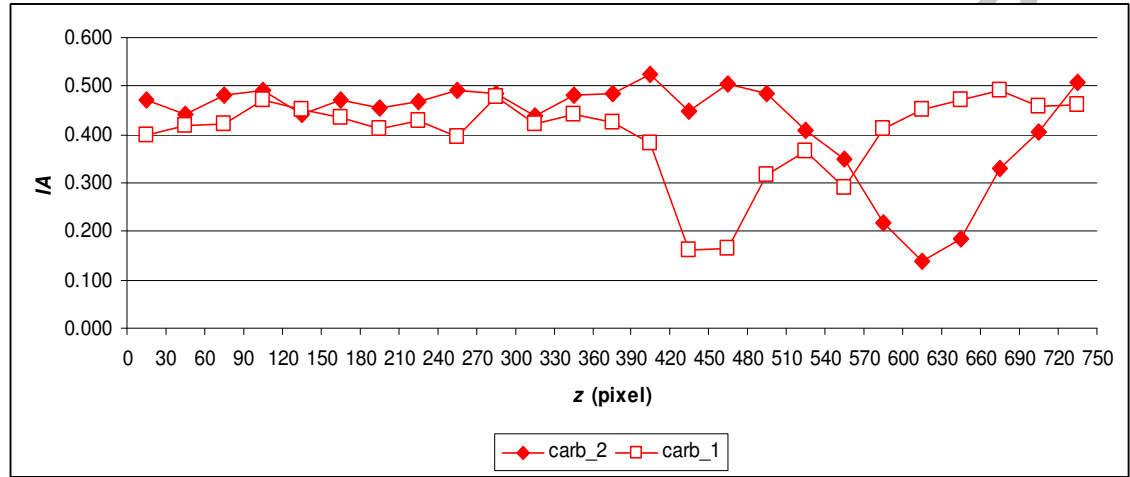


Figure 11: Index of Anisotropy, IA , along z direction (VOIs centre slice position)

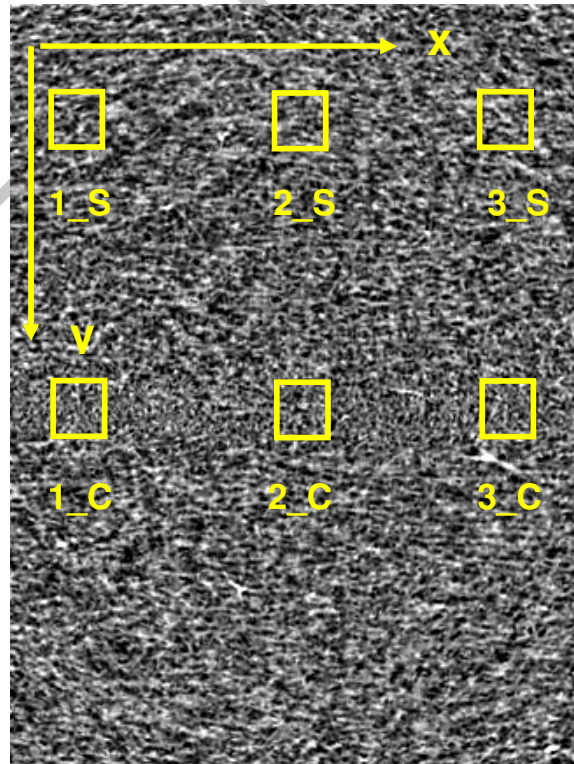


Figure 12: VOIs positions on slice 21.

The proposed method appears to be able to capture the main characteristics of fibre orientation in our samples, as highlighted in Fig.13 where the images obtained by phase-contrast micro-CT are compared to the 3D MIL polar diagrams in two VOIs, 1_C and 1_S, from the core and from the shell regions respectively. The different fibre arrangements are clearly captured by the procedure employed in this work.

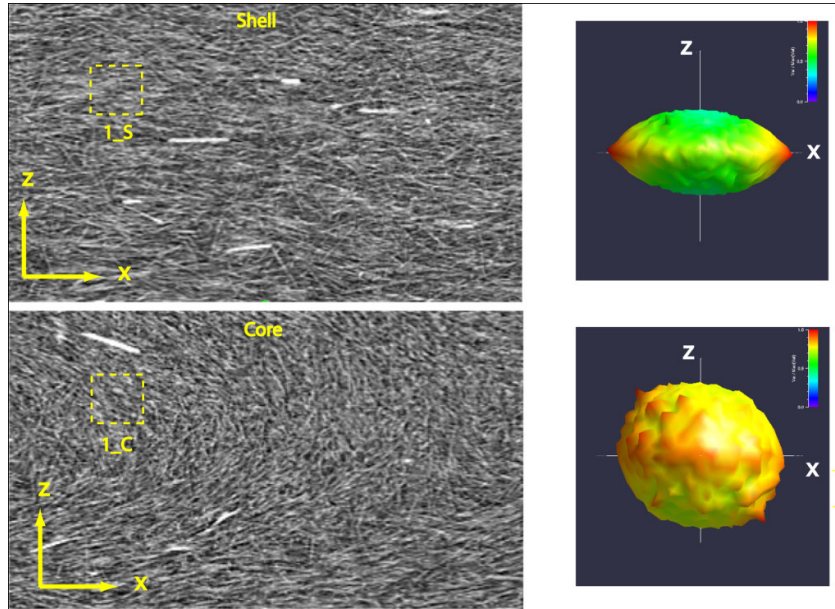


Figure 13: Micro-tomographic images (left) and correspondent MIL polar diagrams (right) in the shell (VOI 1_S) and core (VOI 1_C) regions.

The results of morphological analyses are reported in Tab. 4, where the local variations within a single layer can be appreciated. It can also be seen that anisotropy in the *shell* layer is more strongly marked than in the *core* layer.

Table 4. Index of Anisotropy, IA , in six VOIs having their centre on slice 21 of sample *carb2*.

	I_S	2_S	3_S	I_C	2_C	3_C
IA	0.54	0.48	0.46	0.18	0.14	0.23

By this method, consisting in the analysis of samples of SFRP reconstructed by micro-CT and the evaluation of the components of the MIL fabric tensors, it is possible to derive useful information about the preferred fibre orientation within the VOIs. This work demonstrates that this method, developed for glass fibre reinforced polymers, is also applicable to carbon fibre reinforced polymers. In fact, the limitations deriving from the low difference in absorption index between the matrix and the fibres, could be overcome using PHase Contrast techniques, which enhance small diameter fibre visibility.

5. CONCLUSIONS

High resolution reconstructions of the reinforce short carbon fibre structure within a polymeric matrix could be obtained using X-ray PHase Contrast imaging techniques and morphology identification tools could be applied for anisotropy analyses on the structures thus defined.

Extended regions of the material could be examined, overlapping different tomographies where necessary. The extension to this type of material of the short fibre orientation assessment techniques already introduced by some of the Authors, consented a quantitative analyses of morphology characteristics. In particular, the Index of Anisotropy was evaluated over large portions in two samples extracted from the same

specimen, highlighting the local variations in fibre orientation arrangement induced by the manufacturing process.

ACKNOWLEDGEMENTS

The authors wish to thank Radici Plastics, Italy, for kindly providing the specimens used in this research. This research is funded within the MIUR Prin 2007 program.

REFERENCES

- [1] Zhou Y., Mallick PK. "Fatigue performance of an injection-molded short E-glass fiber-reinforced polyamide 6,6. I. Effects of orientation, holes, and weld line" *Polym. Compos.* 27, 230–237, 2006
- [2] Bernasconi A., Davoli P., Basile A., Filippi A. "Effect of fibre orientation on the fatigue behaviour of a short glass fibre reinforced polyamide-6". *Int J Fatigue.* 29, 199-208, 2007
- [3] Thomason, J.L. "The influence of fibre length, diameter and concentration on the modulus of glass fibre reinforced polyamide 6,6", *Composites Part A*, 39, 1732-1738, 2008
- [4] Nouri H., Meraghni F., Lory P. "Fatigue damage model for injection-molded short glass fibre reinforced thermoplastics", *Int J Fatigue*, 31, 934-942, 2009
- [5] Vincent M., Giroud T., Clarke A., Eberhardt C. "Description and modeling of fibre orientation in injection molding of fiber reinforced thermoplastics", *Polymer*, 46, 6719-6725, 2005
- [6] Dary D., Gilormini P., Régnier G. "Comparison of several closure approximations for evaluating the thermoplastic properties of an injection molded short-fiber composite", *Comp. Sci. Tech.*, 67, 1601-1610, 2007

[7] Bernasconi A., Cosmi F., Dreossi D., “Local anisotropy analysis in injection moulded fibre reinforced polymer composites”, *Comp. Sci. Tech.*, 68, 2574-2581, 2008

[8] Kim E.G, Park J.K, Jo S.H. “A study on fiber orientation during the injection molding of fiber-reinforced polymeric composites (Comparison between image processing results and numerical simulation).” *J Mat Proc Tech*, 111, 225-232, 2001

[9] Liu B.-C., Shen C.-Y., Liu C.-T. “Measurement of fibre orientation in a plaque molded with short fibre reinforced thermoplastics”, *Mat Sc Tech*, Issue suppl. 1, 17-21, 2008

[10] Bay RS, Tucker III CL. “Stereological measurement and error estimates for three-dimensional fiber orientation”, *Polymer Engineering and Science*, 32, 240-253, 1992

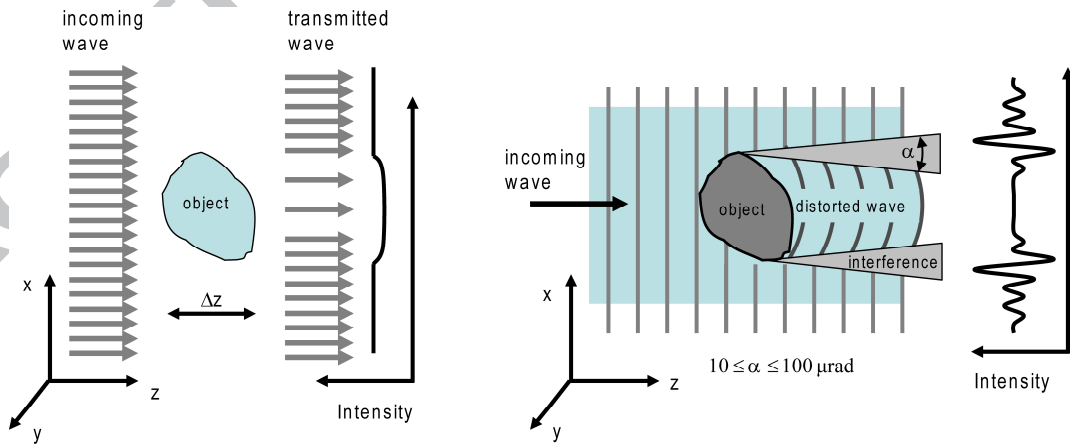
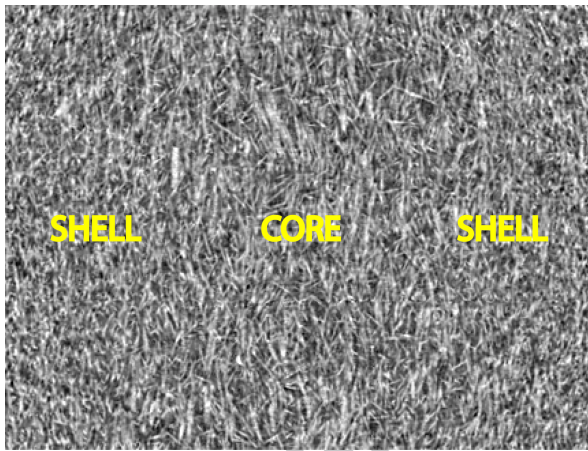
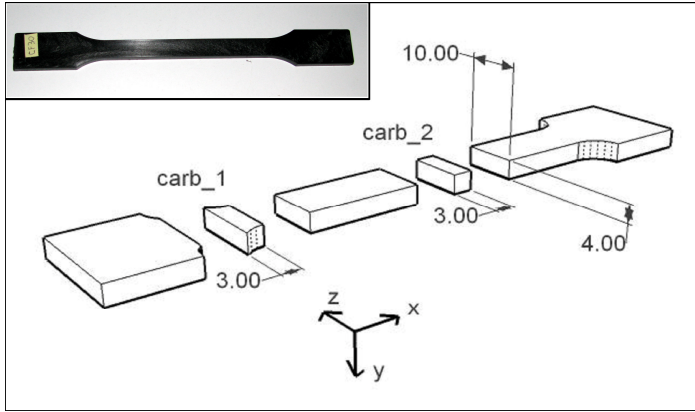
[11] Bernasconi A., Cosmi F., Zappa E., “Combined effect of notches and fibre orientation on fatigue behaviour of short fibre reinforced polyamide”, *Strain*, Published Online: DOI: 10.1111/j.1475-1305.2009.00667.x

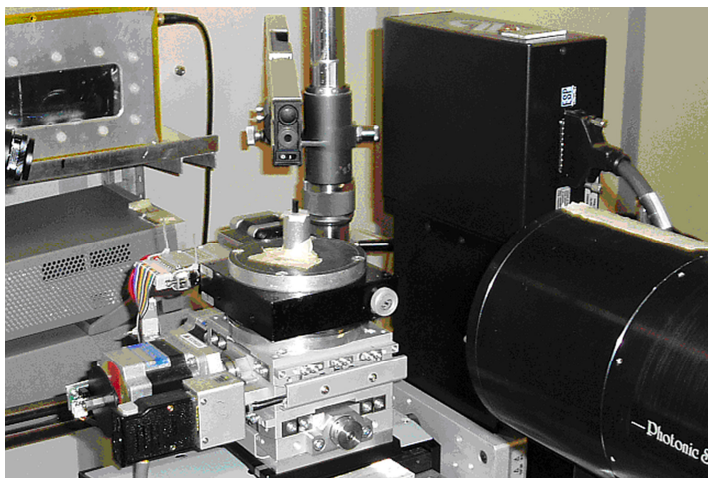
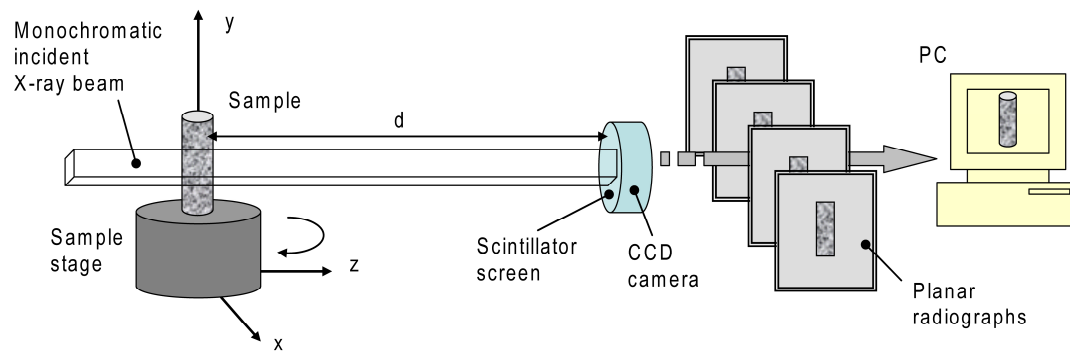
[12] Cosmi F., “Local anisotropy and elastic properties in a short glass fibre reinforced polymer composite”, *Strain*, Published Online: DOI: 10.1111/j.1475-1305.2009.00670.x

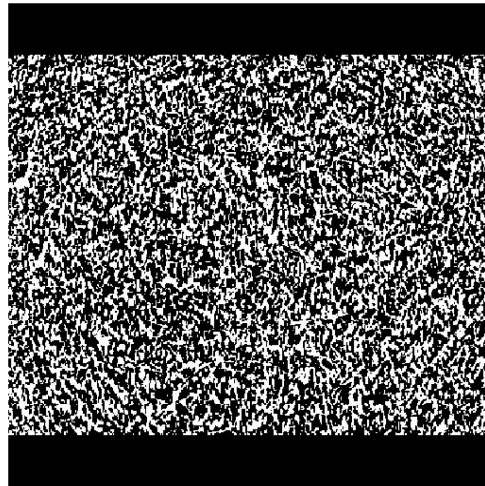
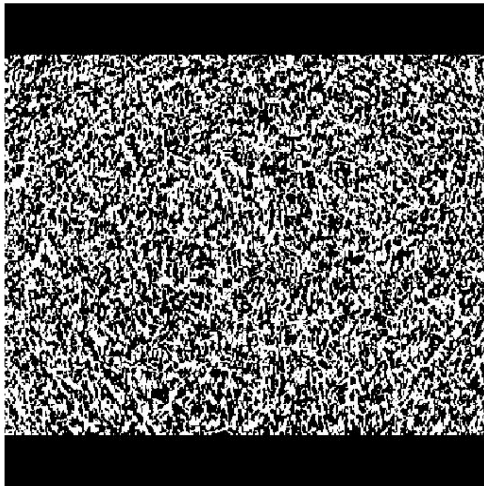
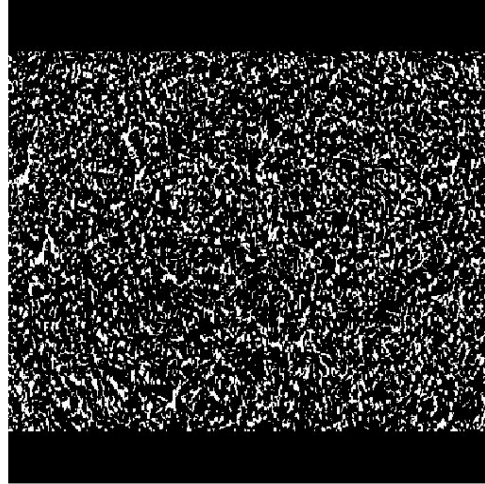
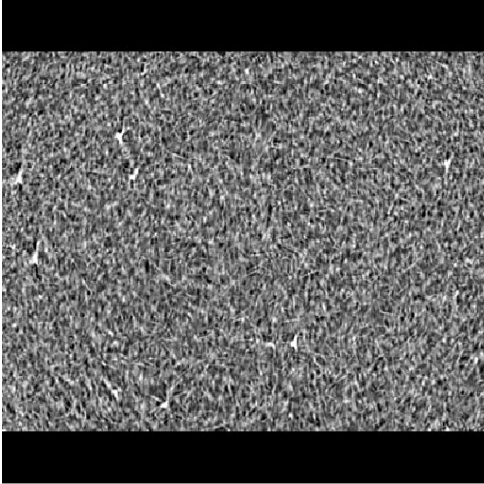
[13] Snigirev A., et al., “On the possibilities of X-ray phase contrast microimaging by coherent high-energy synchrotron radiation”, *Review of Scientific Instruments*, 66, 5486-549, 1995

[14] Requena G., Fiedler G., Seiser B., Degischer P., Di Michiel M., Buslaps T. “3D-Quantification of the distribution of continuous fibres in unidirectionally reinforced composites”, *Composites Part A*, 40, 152-163, 2009

- [15] Martin-Herrero, J., Germain, Ch. “Microstructure reconstruction of fibrous C/C composites from X-ray microtomography”, *Carbon* 45, 1242–1253, 2007
- [16] Fitzgerald R. *Phase-sensitive X-ray imaging*. Available from: <http://websteralt.aip.org/pt/vol-53/iss-7/p23.html>, 2000
- [17] Cloetens P., Barrett R., Baruchel J., Guigay J.P., Schlenker M., “Phase objects in synchrotron radiation hard x-ray imaging”, *J Phys D Appl Phys* 29, 133–146, 1996
- [18] Cloetens P., M. Pateyron-Salomé, J.Y. Buffière, G. Peix, J. Baruchel, F. Peyrin and M. Schlenker (1997), *J. Appl. Phys.* 81, 5878-5785
- [19] Montanari F., *Elettra internal report*, 2003.
- [20] Herman G.T. *Image reconstruction from projections*, Academic Press, New York, 1980
- [21] Abramoff M. D., Magelhaes P.J. & Ram S. J., “Image Processing with ImageJ” *Biophotonics International*, 11, 36-42, 2004
- [22] Luo G.M., Sadegh A.M., Cowin S.C. “The mean intercept length polygons for systems of planar nets”, *J. Mat. Sci.*, 26, 2389-2396, 1991
- [23] Tözeren A., Skalak R. “Does fabric tensor exist for a fabric?” *J. Mat. Sci* 24, 1700-1706, 1989
- [24] Ketcham R.A., Ryan T.M. “Quantification and visualization of anisotropy in trabecular bone”, *J. Microscopy*, 213, 158-171, 2004
- [25] Ryan, T.M., Ketcham, R.A. “The three-dimensional structure of trabecular bone in the femoral head of strepsirrhine primates”. *J. Hum. Evol.* 43, 1-26, 2002
- [26] Quant3D User’s Guide, available from <ftp://ctlab.geo.utexas.edu/Quant3D/>







ACCEPTED

PT

